Viscoelasticity and shear thinning of nanoconfined water

Karan Kapoor, Amandeep, and Shivprasad Patil*

Physics Division, Indian Institute of Science Education and Research, Pune 411008, Maharashtra, India

(Received 30 September 2013; revised manuscript received 5 December 2013; published 8 January 2014)

Understanding flow properties and phase behavior of water confined to nanometer-sized pores and slits is central to a wide range of problems in science, such as percolation in geology, lubrication of future nano-machines, self-assembly and interactions of biomolecules, and transport through porous media in filtration processes. Experiments with different techniques in the past have reported that viscosity of nanoconfined water increases, decreases, or remains close to bulk water. Here we show that water confined to less than 20-nm-thick films exhibits both viscoelasticity and shear thinning. Typically viscoelasticity and shear thinning appear due to shearing of complex non-Newtonian mixtures possessing a slowly relaxing microstructure. The shear response of nanoconfined water in a range of shear frequencies (5 to 25 KHz) reveals that relaxation time diverges with reducing film thickness. It suggests that slow relaxation under confinement possibly arises due to existence of a critical point with respect to slit width. This criticality is similar to the capillary condensation in porous media.

DOI: 10.1103/PhysRevE.89.013004 PACS number(s): 47.61.−k, 07.79.−v, 83.60.Fg, 83.85.Vb

I. INTRODUCTION

Is room temperature water "solid" or "liquid" under nanoconfinement? The question gains significance because water confined to nanoscale hydrophobic and hydrophilic pores and slits is biologically [1–6] and technologically [7–9] important. Force measurement techniques such as the surface force apparatus (SFA) [10–15] and atomic force microscopy (AFM) [16–21] have measured changes in both shear and normal mechanical response of water under molecular level confinement. The conclusions from many of these measurements differ from each other. Here we report measurement of shear response of nanoconfined water at unprecedented shear rates (10^4 to 10^5) s^{-1} with a novel method recently developed by us [22]. Such high shear rates reveal non-Newtonian behavior resulting from slow relaxation of water in the range of 10^{-4} to 10^{-6} s.

We discuss the enabling features of present experiments, which allow viscosity measurements at higher frequencies and shear rates. This experimental scheme has two advantages over the past shear viscosity measurements of water films having thickness of few nm. (1) The spring measuring the viscous drag has high stiffness of 55 000 N/m and yet has a force sensitivity of a few nN [22]. The high stiffness reduces thermal noise in force measurement. (2) The force-measuring spring is out of the liquid and hence has a high resonance frequency (32 kHz) and quality factor (800) [22]. This allows off-resonance measurements with high frequency shear (5 to 25 kHz) and shear rates (10^4 to 10^5 s^{-1}). In previous measurement using AFM, frequencies are restricted to below resonance (≈0.1–2 KHz) of a weak lever and with a low-quality factor (≈5) [18,19]. The ability of measuring shear forces with nN force sensitivity at significantly higher shear frequencies and shear rates has yielded the viscosity measurements of nanoconfined water in a parameter space that so far has not been probed.

II. EXPERIMENTAL

A thin water film of a few nm thickness is confined between an atomically smooth freshly cleaved mica and fiber tip. The tips were prepared by pulling a single-mode fiber in a laser-based fiber puller (Sutter Instrument Co. P2000). They are imaged under ascanning electron microscope (SEM) before use. Figure 1(a) shows an SEM image of a typical tip. The mica is freshly cleaved before the measurement, and the liquid cell is immediately filled with millipore water. Figure 1(b) shows schematic of water confinement. The fiber tip is fixed on one prong of the tuning fork, and the other prong is oscillated off-resonance using a piezo. The current through the electrodes due to asymmetry in prong oscillations is used to measure drag force on the fiber tip [22,23]. A quantitative analysis to determine tip amplitude in bulk (A_0) is given in Appendix B. The tip is oscillated with amplitudes less than 0.5 nm rms in bulk, and separation between tip and sample is varied at a rate of ≈10 nm/s. The shear amplitude is the ratio of oscillation amplitude and separation between tip and sample (A_0/d). We compute the fraction change in drag force offered by confined water ($\delta F/F$) with respect to bulk drag force experienced by the fiber tip: $\delta F/F = k(A_0 - A)/kA_0 = 1 - A/A_0$. A finite phase lag between the piezo drive and oscillations of the tuning fork prong bearing the fiber tip indicates a non-Newtonian viscoelastic response where viscosity is complex, $\eta^* = \eta' - i\eta''$. Maxwell's relaxation time is given by $\tau = (\eta''/\eta')\frac{1}{\omega}$ [22]. The relaxation time of confined water is computed using phase data. The details of this methodology are described in Appendix A.

We remark here that the prong amplitude is always larger in air compared to when the tip is in liquid. As discussed in Ref. [22], the amplitude of the free prong is more than the prong attached to the piezo drive. The current through electrodes is due to this asymmetry in bending. This difference in amplitudes of the two prongs is referred to as differential amplitude $\Delta A = A_1 - A_2$, where A_1 is the amplitude of the prong bearing the tip and A_2 is the amplitude of the prong attached to the piezo drive. The current through electrodes is proportional to ΔA. After immersing the tip in liquid, it experiences a viscous drag force. The amplitude of this prong now decreases slightly and current through the electrode

*Corresponding author: s.patil@iiserpune.ac.in

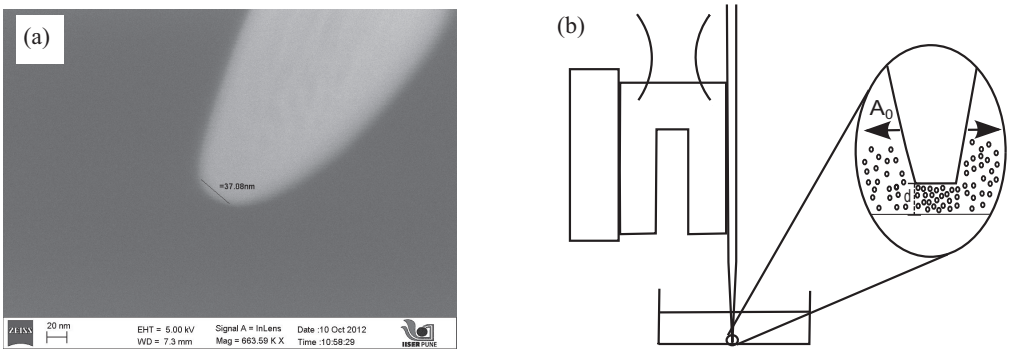

FIG. 1. (a) Scanning electron microscope image of a representative tip used for confinement of water. (b) Schematic of the tuning fork force sensor used to measure shear viscosity of nanoconfined water. A fiber tip is mounted on one prong of a tuning fork, and the other prong is driven with a piezo to provide shear; both prongs of the tuning fork are kept outside water. The current through electrodes is passed through a preamplifier with a gain of 10^7 V/A. A lock-in amplifier measures amplitude and phase of the prong with respect to shear drive provided by piezo. The tip oscillations are less than 0.5 nm rms in bulk.

decreases. This reduction in current is an indicator of drag force offered by the bulk liquid. When the tip further approaches towards the mica surface, the water molecules at the end of the tip become confined and offer a different drag force compared to when the tip was entirely in bulk. The changes in current from its bulk value are a measure of variation in viscosity of nanoconfined water with respect to bulk. We roughly estimate the change in differential prong amplitude using a coupling constant that relates charge accumulation and differential bending of prongs. The actual prong amplitude in bulk is estimated using an independent interferometry measurement. This is described in Appendix A. The change in ΔA when the tip is within a few tens of nm from the mica surface is recorded and used to calculate relative change in drag force due to nanoconfiement

III. RESULTS AND DISCUSSIONS

Figure 2(a)–2(d) shows differential amplitude ΔA, fraction change in drag force ($\delta F/F$), and phase and relaxation

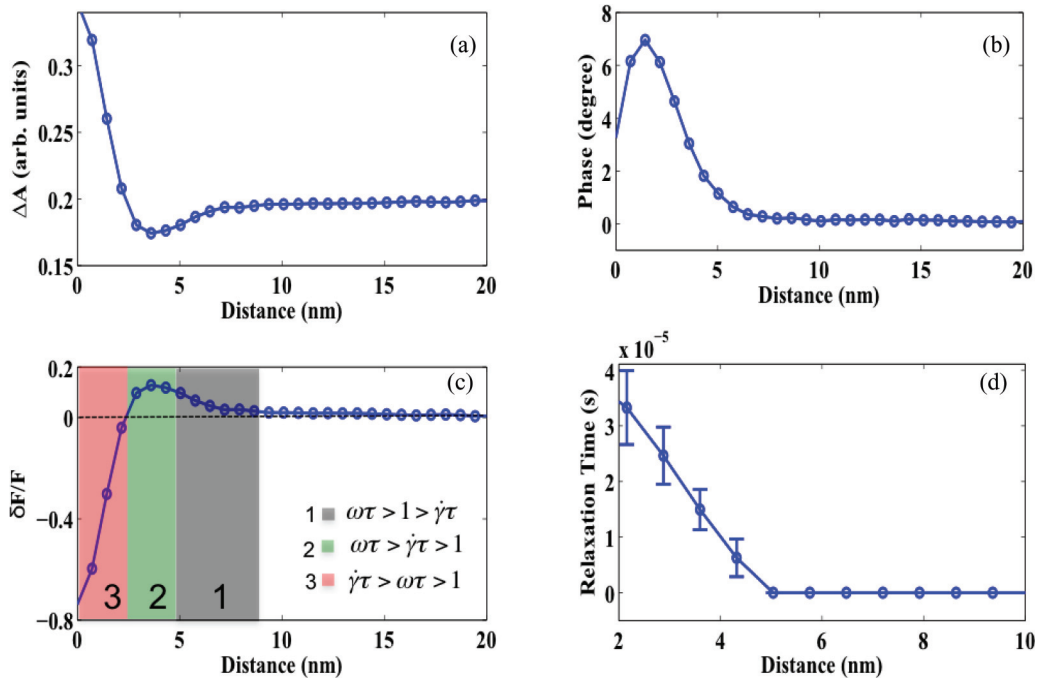

FIG. 2. (Color online) Measurements at 22 kHz shear frequency and approximately 0.2 to 0.3 nm rms amplitude. (a) Differential amplitude $\Delta A = A_1 - A_2$ and (b) phase versus separation. The change in ΔA is inferred from current through electrodes. The change in amplitude is measured using change in current as the tip is approached towards the surface. (c) The fraction change in drag force relative to bulk ($\delta F/F$) computed from data in (a). The prong amplitude when tip is away from the surface is estimated from independent interferometer measurements. The details are provided in Appendix B. Three regions of pure viscoelasticity ($\omega\tau > 1 > \dot{\gamma}\tau$), combined viscoelasticity and shear thinning ($\omega\tau > \dot{\gamma}\tau > 1$), and shear thinning dominating viscoelasticity ($\dot{\gamma}\tau > \omega\tau > 1$), are shown in gray (region marked by 1), green (region marked by 2), and red (region marked by 3), respectively. The dotted line represents the bulk drag force. (d) Relaxation versus separation computed in the region of pure viscoelasticity ($\omega\tau > 1$ but $\dot{\gamma}\tau < 1$).

time as the water film is progressively confined between the fiber tip and mica surface. The measurements are performed at 22 KHz frequency and approximately 0.2–0.3 nm tip oscillation amplitude.

In Fig. 2(c) a finite phase lag at a separation where drag force starts to increase indicates that viscosity is complex under confinement [22]. The mechanical response of the system is now well described by Maxwell's relaxation time. Viscoelasticity appears when a system is sheared with frequency higher than inverse of its relaxation time, $\omega\tau > 1$ [24,25]. In Fig. 2, viscoelasticity starts to appear around a separation of 7.5 nm for shear frequency of 22 kHz. At this separation, $\omega\tau = 1$, which implies $\tau = 8 \times 10^{-6}$ s at 7.5 nm. The shear amplitude γ is ratio of oscillation amplitude and separation. A_0 is shear amplitude and d is separation(see Fig. 1). Typically shear thinning follows viscoelasticity at higher shear rates, and the condition for shear thinning is $\dot{\gamma}\tau > 1$ [25]. At a separation of 7.5 nm and an oscillation amplitude of 0.2 nm, shear amplitude is $\gamma = (A_0/d) = 0.026$. This is purely viscoelastic region in the limit of zero shear amplitude and finite shear frequency. As the separation is reduced shear amplitude as well as relaxation time increase making $\dot{\gamma}\tau > 1$. In Fig. 2(c) this happens around a separation of 2.16 nm and $(\delta F/F)$ starts to decrease, indicating a reduction in drag force. This is the onset of shear thinning behavior. Around this region the condition of $\omega\tau > \dot{\gamma}\tau > 1$ for combined shear thinning and viscoelasticity is satisfied. As tip is approached further towards surface, we see a region where shear thinning dominates viscoelasticity and the net drag force is less than bulk drag force, $\dot{\gamma}\tau > \omega\tau > 1$. This is expected at smaller separations where the shear rate becomes very large for a given frequency.

Figure 2(d) shows relaxation time versus separation computed using phase data. Our methodology to compute relaxation time from phase data is valid only in the viscoelastic region [22]. See Appendix B. For separations below 2.16 nm, the combined viscoelasticity and shear thinning do not allow us to compute relaxation from phase data. At larger separations where $(A_0/d) \ll 1$ and $\dot{\gamma}\tau < 1$, we are in a purely viscoelastic region in the limit of zero shear amplitude. A purely shear thinning regime in the limit of zero frequency where $\omega\tau \ll 1$ but $\dot{\gamma}\tau > 1$ is not possible in our experiments. Such measurements have been reported for dodecane films sheared at strain amplitude of 15 and shear frequencies of few Hz [26].

It is worthwhile comparing our off-resonance shear measurements with previous shear AFM and SFA experiments. Li *et al*. measured the viscoelastic response of nanoconfined water with shear amplitude in the range of 0.1 to 6 and shear frequency around 1 kHz. The shear rate or frequency in these measurement were not high enough to reveal the nonlinear response at separations above 1 nm. In our measurements the frequency and shear rate are in the range of 5 to 25 kHz and 10^4 to 10^6 s^{-1} respectively. This enables measurement of build-up of elastic response at separations larger than 1 nm. Sakuma *et al*. used a modified SFA to include resonance shear measurements [15]. The resonnant response of a part-bearing upper mica sheet is used to infer the viscous and elastic nature of water confined between the two mica surfaces [15]. They have noticed elastic build-up in the shear response of nanoconfined water between silica surfaces from separations as far as 8 nm [27]. This range of separation having a nonlinear response is similar to our measurements. It is important to note that both our measurements and prior shear measurements using AFM employ relatively small strain amplitudes (0.1 to 5) [19] compared to the SFA measurements (10 to 500) [26,27]. The AFM experiments use high frequencies (500 Hz to 2 kHz) whereas shear SFA works with low frequencies (1 to 100 Hz). In particular, our experiments were performed in relatively high strain rates with very small strain amplitudes.

In molecular dynamics (MD) simulations performed by Leng and Cummings [28], the hydrated thin films of water undergo shear thinning at sufficiently high shear rates. They report that films with thickness 1.22 and 0.61 nm are shear thinned whereas thicker films have viscosity close to bulk water. Our experiments show that relaxation time strongly depends on separation, and thinner films can exhibit both viscoelasticity and shear thinning. The shear thinning appears in simulations due to slower rotational dynamics ($\approx 10^{-9}$ s) of water molecules under confinement. Although we are measuring shear response of pure water and our shear rates are orders of magnitude less than these simulations, the parallels between experiments and MD simulations are remarkable. It is noteworthy that water films do exhibit shear thinning in MD simulations, a phenomenon associated with complex non-Newtonian liquids. The physics of combined viscoelasticity and shear thinning is still emerging [29].

The experiment discussed above clearly demonstrates that drag force offered by confined water relative to bulk can increase or decrease depending on shear rate. This underlines the importance of measuring variation in relaxation time of water with slit width (tip-sample separation). Shear thinning and viscoelasticity are more commonplace in complex liquids with a slowly relaxing microstructure. Mixtures such as whipped cream, polymer melts, and colloidal suspensions, typically referred to as soft matter, have a complex viscosity or modulus of rigidity. What is the origin of complex viscosity of pure water under confinement and subsequent viscoelasticity and shear thinning behavior? Here we suggest an analogy between confined liquids and systems close to their critical points. Near a vapor-liquid transition, xenon under microgravity exhibits viscoelasticity and shear thinning [25]. The relaxation rates diverge near this critical point.

In order to probe reasons behind complex viscosity in our experiments, we measured the dependence of relaxation time on slit width. Experiments were performed in a range of shear frequencies (5 to 25 KHz), which allowed us to measure relaxation time of water films with varying slit widths. We used two methodologies to generate a relaxation time verses separation curve: (1) In a purely viscoelastic regime with nearly zero shear amplitudes, we could compute relaxation time from phase data as described in Ref. [22]. This is shown in Fig. 2(d). (2) We know the onset of viscoelastic region from phase and amplitude versus separation data. This onset happens at $\omega\tau = 1$. We can calculate the relaxation time at a separation where onset occurs by taking inverse of shear frequency. The measurement is repeated and the onset for each frequency is noted.

Figure 3 shows a master curve of measurements performed at various frequencies. The relaxation time is computed by the above-mentioned two methods and is plotted versus separation in one single curve. The points computed using

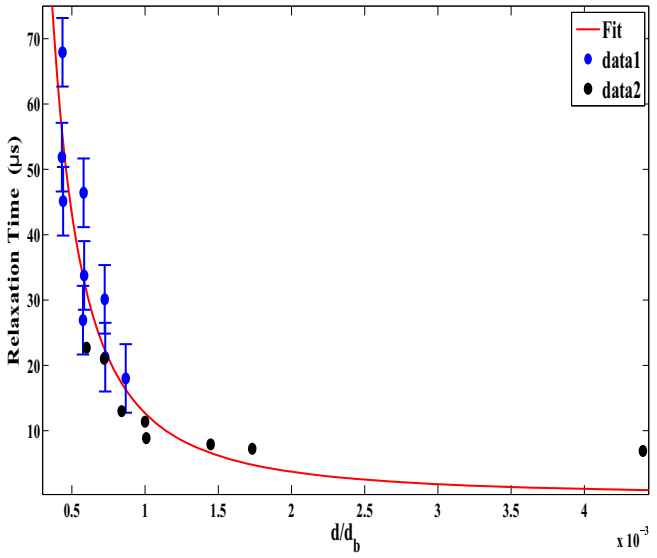

FIG. 3. (Color online) Relaxation versus separation master curve. Two methodologies are used to compute relaxation time as described in the text. Black circles without error bars are points calculated using $\omega\tau = 1$; blue circles with error bars are points calculated using method in Ref. [21]. The line is a fit with equation $\tau/\tau_{\text{bulk}} = (d/d_{\text{bulk}})^{-\alpha}$, $\alpha = 1.77 \pm 0.5$, and d_{bulk} is 5 μm assuming τ_{bulk} to be 62 ps. Errors in estimating relaxation using method 1 originate from poor determination of spring constant k_2.

methods 1 and 2 are plotted in different colors. We fit a power law to this data $\tau/\tau_{\text{bulk}} = (d/d_{\text{bulk}})^{-\alpha}$. Here τ_{bulk} is bulk relaxation time corresponding to separation d_{bulk}. The fit yields exponent $\alpha = 1.77 \pm 0.5$, and d_{bulk} takes value of 5 μm for $\tau_{\text{bulk}} = 62$ ps. The divergence of relaxation time with film thickness is striking. The divergence and critical exponents characterizing a universality class are typical to a second order phase transition [30]. It implies that by reducing film thickness we are pushing the system towards a critical point. Although a shift in transition temperature under confinement is very well known [31], it is unlikely that vapor-water critical point comes close to room temperature. Indeed, the freezing and melting point shifts for water in porous silica are reported to be only by few K [32]. Evans and co-workers have predicted criticalities related to capillary condensation in the case of liquids under nanoconfinement [33,34]. They have argued that under confinement the liquid-wall interaction becomes stronger relative to liquid-liquid interaction, increasing effective chemical potential. At a critical separation the coexistence of two liquid states having different density profiles vanishes [33]. Despite the lack of detailed calculations for water, it can be argued that slow relaxation under confinement occurs due to critical slowdown near a second order phase transition from a low density bulk-like phase to a very high density "dynamically solidified phase" described in Ref. [18]. This argument needs further experimental investigation and theoretical support. Critically slowed confined water also explains shear response at separations as large as 20 nm in our experiments at high shear frequencies.

Water (polar and associative liquid) is thought to behave differently under confinement compared to other organic liquids (nonpolar, nonassociative) [13]. Evidence for shear thinning in case of water suggests a similarity in behavior for water and dodecane [26]. This similarity also exists in normal mechanical response of water and octamethylcyclotetrasiloxane [18,35]. Further, measurement of relaxation together with optical measurements that may enable monitoring of critical scattering will shed light on the nature of critical phenomena associated with nanoconfined liquids.

In summary, we have measured rheological response of nanoconfined water with unprecedented shear rates. The measurements reveal viscoelasticity and shear thinning at confining separations as large as few nm. The divergence of relaxation with reducing separation hints at a possible criticality in nanoconfined water.

ACKNOWLEDGMENTS

The work is funded by a Department of Science and Technology nanomission grant (SR/NM/NS- 84/2009). The authors would like to thank Arijit Bhattacharyay for useful discussions.

APPENDIX A: ESTIMATION OF SHEAR AMPLITUDE

Shear amplitude is given by A_0/d, where A_0 is amplitude of tip oscillation and d is separation between tip and the surface. To estimate shear amplitude we need to obtain zero of the separation in our measurement and amplitude of the tuning fork prong when it is far from the surface. In the following we discuss methods of estimating these and possible errors involved.

1. Determination of zero of the separation *d*

Mechanical response of confined liquids is measured using two techniques: a surface force apparatus (SFA) and atomic force microscopy (AFM). SFA measures separation of atomically smooth confining walls using interferometry. These measurements typically estimate separation between surfaces with 0.4 nm accuracy ($\approx$ thickness of a water monolayer) [12,13]. In the case of AFM, there is no such independent measurement of separation, and zero of the separation is usually inferred from a sudden change in a cantilever's normal static deflection upon touching the surface [17,18]. However, it is not clear if the first surface-bound layer of water moves out of the approaching tip and surface. In our measurements vertical stiffness is nearly infinite, and we cannot measure vertical deflections. We assume that the first layer of water is bound to the surface and is not squeezed out in approach. It has the same shear response under varying loads [12]. We can assign zero of the separation to a point where amplitude stops varying any further. It is seen in experiments that after the initial decrease and increase, the amplitude stays constant upon further approach. We treat this as zero of separation in our measurement, and it has an accuracy of 0.4 nm. However, the step size in our separation measurement is 0.7 nm. There will be an error of 0.7 nm in determining the point at which the amplitude remains constant. Our step size is limited by measurement bandwidth required to pick up signal from noise using lock-in amplifiers. This can be improved further with better signal-to-noise ratio in preamplifier.

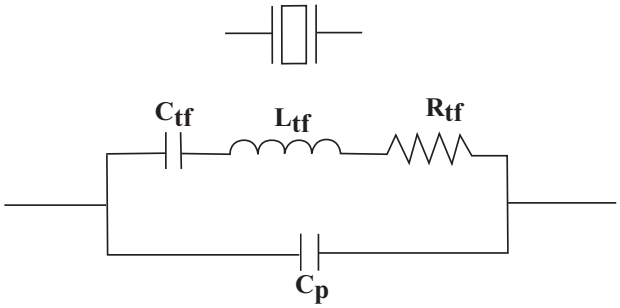

FIG. 4. Equivalent electrical circuit for tuning fork.

2. Measurement of free tip oscillation amplitude A_0

Accurate measurement of shear amplitude is important in rheology for identifying different regions of liquid's complex behavior. In present experiments the current through prongs is used to measure differential amplitude. The actual tip amplitude is not possible to determine; instead we measure off-resonance prong amplitude using an interferometer and relate this to current through coupling constant. This gives us a rough idea of the amplitude of tuning fork prong when it is immersed in liquid. The change in amplitude is estimated using change in current as the tip approaches the mica surface. The tuning fork equivalent electrical circuit is shown in Fig. 4. Here C_p represents stray parasitic capacitance due to electrical contacts made to the electrodes. In our experiments we put a 10μF capacitance in series to null this capacitance, but it never compensates stray capacitance completely. The current through electrodes has two contributions: (1) current due to asymmetric bending of prongs, which depends on amount of bending and the coupling constant ε, the charge accumulated per unit bending, and (2) the current through the uncompensated parasitic capacitance C_p:

$$i = \varepsilon\omega(A_1 - A_2) + \omega C_p, \qquad \text{(A1)}$$

where ε is a coupling constant, ω is frequency of operation, and $(A_1 - A_2)$ is the difference in bending between two prongs or differential amplitude. For on-resonance operation, the first term is dominant, and tuning fork amplitude is measured using current through electrodes [23].

For off-resonance operation, the piezo drive and both prongs move in phase and by an equal amount. As mentioned in Ref. [22] we found that there is a slight asymmetry in bending at off-resonance, also supported by COMSOL simulations. This causes a small amount of current to flow through the electrodes; however, current due to parasitic capacitance overwhelms this value. Therefore, it is not possible to determine free amplitude from current alone in off-resonance operation. Although we perform our measurements in off-resonance, one of the prongs experiences the drag force due to immersion of the tip attached to it in liquid. The term involving $(A_1 - A_2)$ is a measure of drag force acting on the fiber tip. The term involving C_p remains constant when the tip is immersed in liquid or approaches the surface. We therefore use change in current to measure change in drag force, while amplitude in bulk is estimated from independent interferometry measurements. The amplitude of the prong bearing the tip is much larger when the tip is in air compared to when the tip is immersed in liquids. The change in amplitude when the tip approaches the surface is inferred from changes in electrode currents. Figure 5 shows a schematic of this interferometer measurement. Light from 1350 nm diode laser is passed through a 2×2 coupler. Part of this split light goes

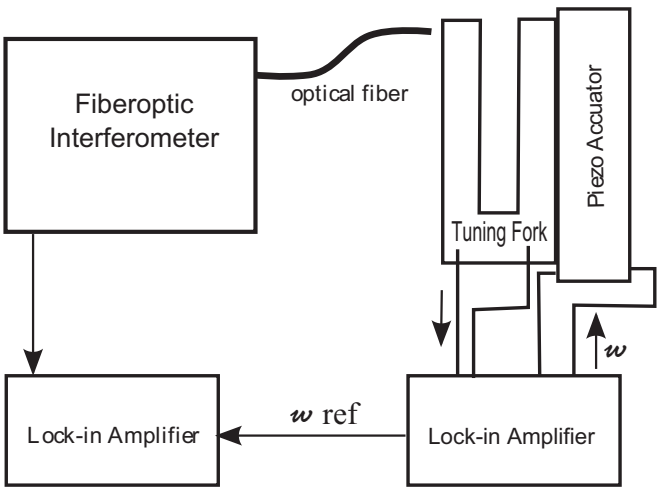

FIG. 5. Schematic of interferometer to measure the free oscillation amplitude away from the surface.

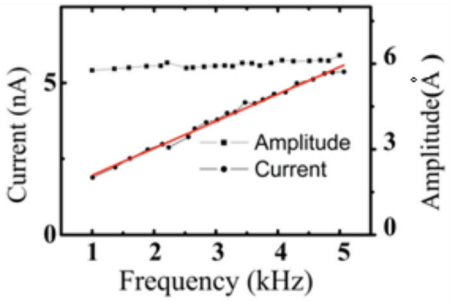

FIG. 6. (Color online) Current through electrodes and the actual amplitude of one prong of the tuning fork. Current follows Eq. (A1). Most of the current is due to parasitic capacitance in off-resonance condition. The variation in current due to asymmetric prong bending is small but measurable while performing force measurements.

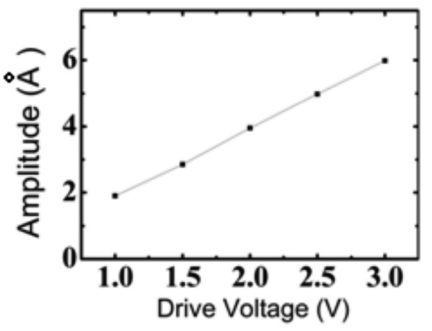

FIG. 7. The drive amplitude measured using an interferometer with different drive voltages on the piezo. In all our experiments we used a drive of 0.5 to 1 V.

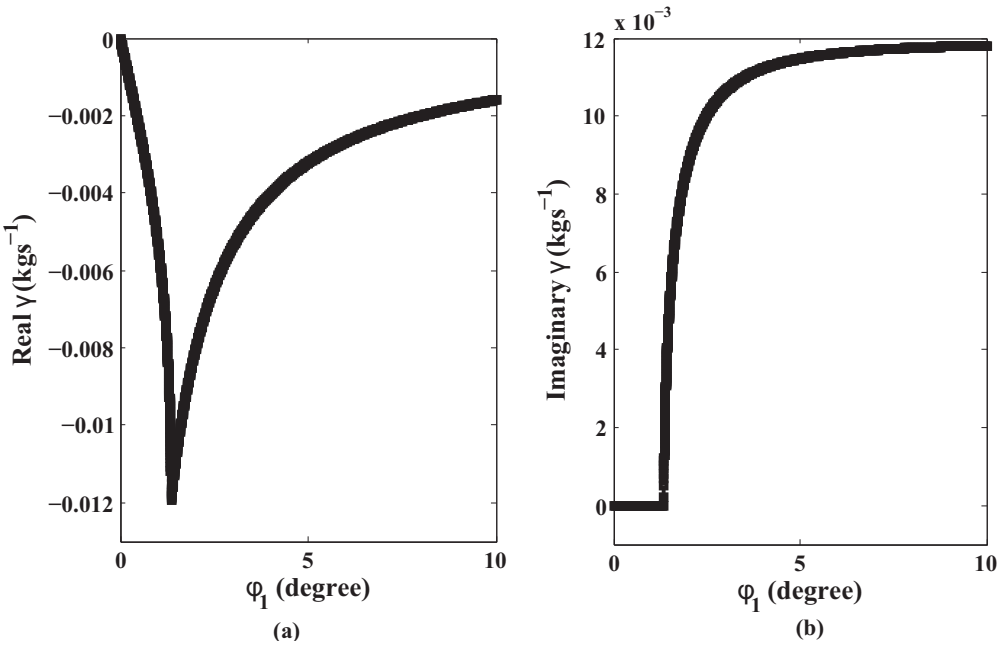

FIG. 8. The real and imaginary parts of damping coefficients with phase ϕ_1. The value of phase ϕ_1 for which the viscosity turns complex depends on k_2.

to the fiber having a half mirror coated on its other end. This end of the fiber forms a Fabry-Perot etalon with the surface of one prong of the tuning fork. The reflected light from the half mirror and tuning fork surface interferes to produce a pattern on the photodiode. The separation between fiber end and tuning fork arm is fixed with a feedback control. Oscillation amplitudes are determined from slope at this locked point on interference pattern.

Figure 6 shows measurement of tuning fork amplitude using an interferometer and current through electrodes versus frequency. As expected the amplitude signal measured using the interferometer remains constant and is equal to amount of drive provided. This drive is measured by positioning the fiber of the interferometer on the piezo used for the drive. The current due to parasitic capacitance linearly increases with frequency. We used resonance conditions to determine the coupling constant $\varepsilon = 36\ \mu$C/m, since on-resonance the contribution due to second term is not significant. We use ε to estimate the expected current change due to asymmetric bending in the tuning fork.

COMSOL simulations of a tuning fork used in our experiments show that for higher frequencies the free prong of the tuning fork has around 10% more amplitude compared to one bound to the piezo driver. This is also taken into account while determining free amplitude of the shear.

We measure drive amplitude of the piezo by placing the interferometer fiber on a mirror mounted on the piezo. Figure 7 shows calibration of piezos used for a shear drive.

APPENDIX B: CALCULATION OF RELAXATION TIME FROM PHASE DATA

Typically a phase relationship between stress and strain gives information about the type of mechanical response the system offers under oscillatory shear. Hookean solids have zero phase between stress and strain, Newtonian liquids have 90° phase, and for a viscoelastic system the phase lag is in between these two extremes. The stress-strain relationship for viscoelastic materials is given by $\sigma = G^*\gamma$, where σ is stress, γ is strain, and $G^* = G' + iG''$ is complex modulus of rigidity. Similarly complex viscosity is defined as $\eta = \eta' - i\eta''$. Maxwell's relaxation time is given by $\tau = (G'/G'')1/\omega = (\eta''/\eta')1/\omega$, where ω is shear frequency [24]. In our experiments we measure change in drag force relative to bulk upon confinement. After solving equations of motion for the coupled oscillator we plot solutions as described in Ref. [22]. Using reasonable values of k_1 and k_2 in these solutions, phase of tuning fork prong and the fiber tip is plotted versus damping coefficient. The phase of tuning fork prong ϕ_1 with respect to the piezo driver converges to zero. This is expected since both are outside liquid and driven off resonance. For a fiber tip, which is immersed in liquid the phase difference ϕ_2 converges to 90°. This is consistent with conventional physical picture of Newtonian liquids. The plots validate our model and solutions we obtained after solving it (see Ref. [22]). The solution for phase ϕ_1 of the tuning fork prong is given below. Note that this is the phase we are experimentally able to measure, and not fiber tip phase ϕ_2:

$$\phi_1 = \tan^{-1}\left(\frac{-k_2^2\gamma\omega}{\{(k_1+k_2-m_1\omega^2)[\gamma^2\omega^2 - m_2\omega^2(k_2-m_2\omega^2)] + k_2(k_1-m_1\omega^2)(k_2-m_2\omega^2)\}}\right). \quad \text{(B1)}$$

The damping coefficient becomes complex at a certain value of phase ϕ_1 (see Fig. 8). This onset depends on k_1, k_2, m_1, and m_2. Of these four parameters, k_1, m_1, and m_2 are accurately determined. The value of k_2 is estimated from tip length protruding from the tuning fork prong and using COMSOL to determine its eigenfrequency. A complex damping coefficient indicates complex viscosity. Relaxation can now be determined by measuring ϕ_1 as the tip approaches the surface and determining real (γ') and imaginary (γ'') parts of the damping coefficient, $\tau = (\gamma''/\gamma')1/\omega = (\eta''/\eta')1/\omega$.

It should be noted here that error in estimating relaxation is primarily due to error in k_2. This error will be systematic and will not change the power law behavior or the exponent presented in Fig. 3. The absolute values of relaxation may have errors. These errors are shown as error bars in Fig. 3. The onset of viscoelastic behavior with respect to separation is marked by a finite phase difference between the piezo driver and tuning fork prong. As expected, weaker fiber tips are more sensitive to both force as well as relaxation time measurements.

[1] O. Beckstein and M. S. P. Sansom, Phys. Biol. **1**, 42 (2004).
[2] Y. Zhou, J. H. Morais-Cabral, A. Kaufman, and R. MacKinnon, Nature (London) **414**, 43 (2001).
[3] M. S. P. Sansom and P. C. Biggin, Nature (London) **414**, 156 (2001).
[4] S. Granick and C. Bae, Science **322**, 1477 (2008).
[5] A. Fernandez, Phys. Rev. Lett. **108**, 188102 (2012).
[6] J. L. Finney, Faraday Discuss. Chem. Soc. **103**, 1 (1996).
[7] R. Szoszkiewicz and E. Riedo, Phys. Rev. Lett. **95**, 135502 (2005).
[8] J. N. Israelachvili, P. M. McGuiggan, and A. M. Homola, Science **240**, 189 (1988).
[9] M. Scherge, X. Li, and J. A. Schaefer, Tribol. Lett. **6**, 215 (1999).
[10] J. N. Israelachvili and R. M. Pashley, Nature (London) **306**, 249 (1983).
[11] R. G. Horn, D. T. Smith, and W. Haller, Chem. Phys. Lett. **162**, 404 (1989).
[12] Y. Zhu and S. Granick, Phys. Rev. Lett. **87**, 096104 (2001).
[13] U. Raviv, P. Laurat, and J. Klein, Nature (London) **413**, 51 (2001).
[14] U. Raviv and J. Klein, Science **297**, 1540 (2002).
[15] H. Sakuma, K. Otsuki, and K. Kurihara, Phys. Rev. Lett. **96**, 046104 (2006).
[16] S. J. O'Shea, M. E. Welland, and T. Rayment, Appl. Phys. Lett. **60**, 2356 (1992).
[17] S. Jeffery, P. M. Hoffmann, J. B. Pethica, C. Ramanujan, H. Ozgur Ozer, and A. Oral, Phys. Rev. B. **70**, 054114 (2004).
[18] S. H. Khan, G. Matei, S. Patil, and P. M. Hoffmann, Phys. Rev. Lett. **105**, 106101 (2010).
[19] T. D. Li and E. Riedo, Phys. Rev. Lett. **100**, 106102 (2008).
[20] T. D. Li, J. Gao, R. Szoszkiewicz, U. Landman, and E. Riedo, Phy. Rev. B **75**, 115415 (2007).
[21] A. Ulcinaset *et al.*, Langmuir **27**, 10351 (2011).
[22] K. Kapoor, V. Kanwade, V. Shukla, and S. Patil, Rev. Sci. Instrum. **84**, 025101 (2013).
[23] F. J. Giessibl, Appl. Phys. Lett. **76**, 1470 (2000).
[24] R. G. Larson, *The Structure and Rheology of Complex Liquids* (Oxford University Press, New York, 1999), pp. 3–60.
[25] R. F. Berg, M. R. Moldover, M. Yao, and G. A. Zimmerli, Phys. Rev. E. **77**, 041116 (2008).
[26] S. Granick, Science **253**, 1374 (1991).
[27] M. Kasuya *et al.*, J. Phys. Chem. C **117**, 13540 (2013).
[28] Y. Leng and P. T. Cummings, Phys. Rev. Lett. **94**, 026101 (2005).
[29] P. Das and J. K. Bhattacharjee, Phys. Rev. E. **71**, 036145 (2005).
[30] P. C. Hoenberg and B. I. Halperin, Rev. Mod. Phys. **49**, 435 (1977).
[31] H. Nakanishi and M. E. Fisher, J. Chem. Phys. **78**, 3279 (1983).
[32] S. Jahnert *et al.*, Phys. Chem. Chem. Phys. **10**, 6039 (2008).
[33] R. Evans, U. M. B. Marconi, and P. Tarazona, J. Chem. Phys. **84**, 2376 (1986).
[34] R. Evans, J. Phys.: Condens. Matter. **2**, 8989 (1990).
[35] S. Patil, G. Matei, A. Oral, and P. M. Hoffmann, Langmuir **22**, 6485 (2006).